A&A 567, A4 (2014)
DOI: 10.1051/0004-6361/201322959

Astronomy & Astrophysics

Refining the asteroseismic model for the young δ Scuti star HD 144277 using HARPS spectroscopy⋆

K. Zwintz[1], T. Ryabchikova[2], P. Lenz[3], A. A. Pamyatnykh[2,3,4], L. Fossati[5], T. Sitnova[2,6], M. Breger[7], E. Poretti[8], M. Rainer[8], M. Hareter[4], and L. Mantegazza[8]

[1] Instituut voor Sterrenkunde, K. U. Leuven, Celestijnenlaan 200D, 3001 Leuven, Belgium
e-mail: konstanze.zwintz@ster.kuleuven.be
[2] Institute of Astronomy, Russian Academy of Sciences, Pyatnitskaya Str. 48, 109017 Moscow, Russia
[3] Copernicus Astronomical Centre, Bartycka 18, 00-716 Warsaw, Poland
[4] University of Vienna, Institute of Astronomy, Türkenschanzstrasse 17, 1180 Vienna, Austria
[5] Argelander-Institut für Astronomie der Universität Bonn, auf dem Hügel 71, 53121 Bonn, Germany
[6] Moscow M.V. Lomonosov State University, Sternberg Astronomical Institute, Universitetskii pr. 13, 119992 Moscow, Russia
[7] Dept. of Astronomy, University of Texas at Austin, Austin TX 78712, USA
[8] INAF – Osservatorio Astronomico di Brera, Merate, Italy

Received 31 October 2013 / Accepted 5 May 2014

ABSTRACT

Context. HD 144277 was previously discovered by Microvariability and Oscillations of Stars (MOST) space photometry to be a young and hot δ Scuti star showing regular groups of pulsation frequencies. The first asteroseismic models required lower than solar metallicity to fit the observed frequency range based on a purely photometric analysis.
Aims. The aim of the present paper is to determine, by means of high-resolution spectroscopy, fundamental stellar parameters required for the asteroseismic model of HD 144277, and subsequently, to refine it.
Methods. High-resolution, high signal-to-noise spectroscopic data obtained with the HARPS spectrograph were used to determine the fundamental parameters and chemical abundances of HD 144277. These values were put into context alongside the results from asteroseismic models.
Results. The effective temperature, $T_{\rm eff}$, of HD 144277 was determined as $8640\,^{+300}_{-100}$ K, $\log g$ is 4.14 ± 0.15 and the projected rotational velocity, $\upsilon \sin i$, is 62.0 ± 2.0 km s^{-1}. As the $\upsilon \sin i$ value is significantly larger than previously assumed, we refined the first asteroseimic model accordingly. The overall metallicity Z was determined to be 0.011 where the light elements He, C, O, Na, and S show solar chemical composition, but the heavier elements are significantly underabundant. In addition, the radius of HD 144277 was determined to be 1.55 ± 0.65 $R_\odot$ from spectral energy distribution fitting, based on photometric data taken from the literature.
Conclusions. From the spectroscopic observations, we could confirm our previous assumption from asteroseismic models that HD 144277 has less than solar metallicity. The fundamental parameters derived from asteroseismology, $T_{\rm eff}$, $\log g$, $L/L_\odot$ and $R/R_\odot$ agree within one sigma to the values found from spectroscopic analysis. As the $\upsilon \sin i$ value is significantly higher than assumed in the first analysis, near-degeneracies and rotational mode coupling were taken into account in the new models. These suggest that HD 144277 has an equatorial rotational velocity of about 80 km s^{-1} and is seen equator-on. The observed frequencies are identified as prograde modes.

Key words. stars: variables: delta Scuti – stars: oscillations – stars: individual: HD 144277 – stars: fundamental parameters – techniques: photometric – asteroseismology

1. Introduction

High-precision time-series photometry obtained by the Microvariability and Oscillations of Stars space telescope (MOST; Walker et al. 2003) during two consecutive years discovered δ Scuti pulsations in HD 144277 (Zwintz et al. 2011; Paper I, hereafter). The twelve independent pulsation frequencies identified lie in four distinct groups, i.e., they show regular frequency patterns. The first asteroseismic analysis was based on limited additional knowledge of the physical parameters of HD 144277. The star was only known to have a spectral type of A1V with a respective effective temperature of 9230 K (both taken from the Tycho-2 Spectral Type Catalog; Wright et al. 2003), and a parallax of 7.00 ± 5.59 mas (Kharchenko & Roeser 2009). No spectroscopic data were available and the location of HD 144277 at the hot border of the δ Scuti instability strip was determined by dedicated Strömgren photometry (see Paper I for more details).

The asteroseismic analysis conducted in Paper I found evidence of two radial modes of sixth and seventh overtones under the assumption of slow rotation. The models calculated in Paper I needed slightly less than solar metallicity and a moderate enhancement of the helium abundance compared to the standard solar chemical composition.

With the lack of high-resolution spectroscopy for HD 144277, it was not possible to test if the non-solar abundances required from asteroseismology for the excitation of the observed δ Scuti frequencies could also be found in

⋆ This work is based on ground-based observations made with the 3.6 m telescope at La Silla Observatory under the ESO Large Programme LP185.D-0056.

the atmosphere of the star. The asteroseismic models would of course also be different, if the $\upsilon \sin i$ were significantly larger than assumed in Paper I. We obtained high-resolution spectra for HD 144277 in order to test the validity of the first asteroseismic models and the assumptions needed to explain the observed frequencies.

We present here the results of our spectral analysis for HD 144277 that lead to a refinement of the asteroseismic models first presented in Paper I.

2. High-resolution spectroscopy: observations and data reduction

Fundamental parameters and abundances for HD 144277 were determined from spectra obtained during five nights between 2011 June 28 and July 3 with the HARPS spectrograph (Mayor et al. 2003) at the 3.6 m telescope of ESO La Silla Observatory. HD 144277 was used as a backup target for the ESO LP185.D-0056 to extend the physical scenario of the δ Sct stars observed with CoRoT. In the adopted EGGS configuration the fiber-fed high-resolution échelle spectrograph has a resolving power of 80 000. Each spectrum covers the wavelength range of 3781–6913 Å.

The 18 single spectra of HD 144277 were observed for exposure times of 1100 (15 spectra), 1200 (two spectra) and 1300 (one spectrum) seconds and have mean pixel-by-pixel signal-to-noise ratios (S/N) between 143 and 248 calculated in the wavelength range of 5805 to 5825 Å. The HARPS spectra, in the adopted configuration, cover the hydrogen Balmer lines Hα, Hβ, Hγ, Hδ, and Hϵ. Since the 18 single spectra were obtained during five different nights and since the pulsation periods discovered earlier are shorter than 24 min, the data could not be used as a spectroscopic time series to study line profile variations. Figure 1 shows that both the radial velocity variations and the line profile variations are much smaller than the rotational broadening. The 18 single spectra were therefore combined to increase the S/N of the combined spectrum that then amounts to 363 computed again in the wavelength range of 5805 to 5825 Å.

The spectra were reduced using both the ESO pipeline and a semi-automatic MIDAS pipeline (Rainer 2003). They were then normalized by fitting a low-order polynomial to carefully selected continuum points. The resulting normalized combined high-resolution spectrum was thereafter used to determine the fundamental stellar parameters presented in this article.

3. Atmospheric parameters determination and abundance analysis

The starting values for determining the fundamental parameters and chemical abundances of HD 144277 were taken from multicolor photometry. For HD 144277 Strömgren colors (Paper I) without β-parameter, and usual broad-band photometric data are available. With three different calibrations of Strömgren photometric indices (Moon & Dworetsky 1985; Balona 1994; Ribas et al. 1997) included in the TEMPLOGG package (Kaiser 2006), and with a proper range of assumed β-parameters, we estimated $T_{\rm eff} = 8800 \pm 150$ K, $\log g = 3.9$–4.1, and metallicity M of -0.28 from photometry.

A comparison between the observed spectrum of HD 144277 and the synthetic spectrum, calculated for an atmospheric model with the above mentioned parameters, shows a rather high rotational velocity, and, as a consequence, strong line-blending. This led us to use spectral synthesis and employ the SME

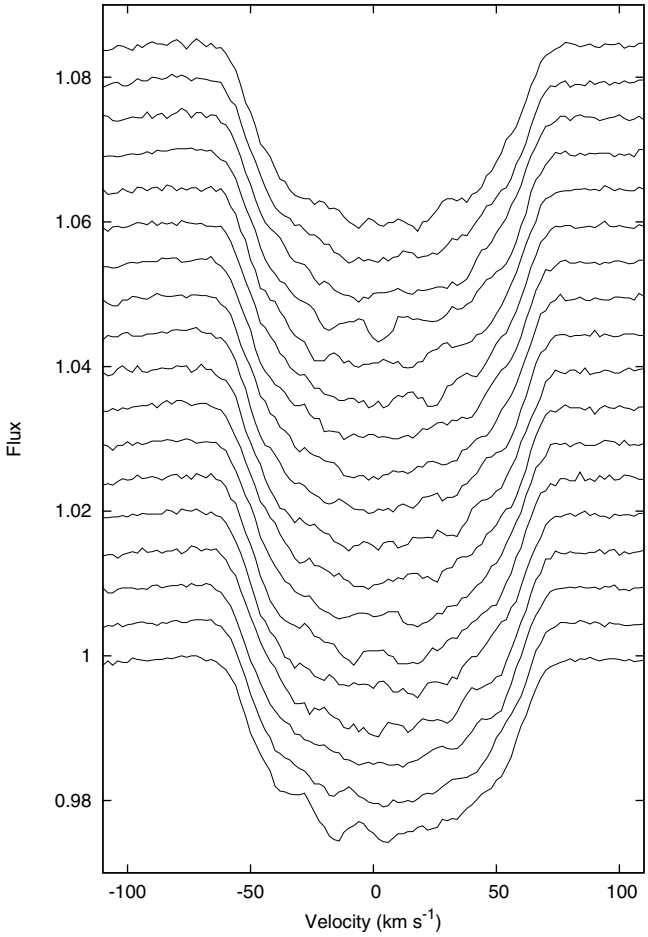

Fig. 1. Mean line profiles for each of the 18 single spectra obtained for HD 144277 on different nights. Spectral intensities (in continuum units) on the y-axis are arbitrarily shifted for better visibility. Spectra are in chronological order from bottom to top.

(Spectroscopy Made Easy) package to derive the atmospheric parameters for HD 144277. The SME software was developed by Valenti & Piskunov (1996) and, for example, was successfully applied to determine the atmospheric parameters of FGK stars (Valenti & Fischer 2005). SME allows to derive effective temperature, surface gravity, overall metallicity, individual element abundances, and the microturbulent, macroturbulent, rotational, and radial velocities of a star by fitting synthetic spectra to the observed ones. Spectral synthesis calculations may be performed for different grids of model atmospheres and are interpolated between the grid nodes. We used a model grid calculated with the LLMODELS stellar model atmosphere code (Shulyak et al. 2004) for microturbulent velocity $\upsilon_{\rm mic} = 2.0$ km s^{-1}, which ranges from 4500–22 000 K in effective temperature, from 2.5–5.0 dex in surface gravity, and from -0.8–0.8 dex in metallicity (see Table 5 in Tkachenko et al. 2012). The corresponding steps are 0.1 in $\log g$, 0.1 dex in metallicity, 100 K in the effective temperature region from 4500–10 000 K and 250 K for higher $T_{\rm eff}$ values.

The following spectral regions were chosen for the fitting procedure of HD 144277: 4140–4410 Å, 4411–4705 Å, 4750–4963 Å, 4963–5298 Å, 5257–5620 Å, 6100–6250 Å, 6340–6465 Å and 6480–6580 Å. These ranges include the three Balmer lines Hα, Hβ, and Hγ. Atomic parameters were extracted from the Vienna Atomic Line Database (VALD). We chose three different steps to derive the star's parameters: (i) we

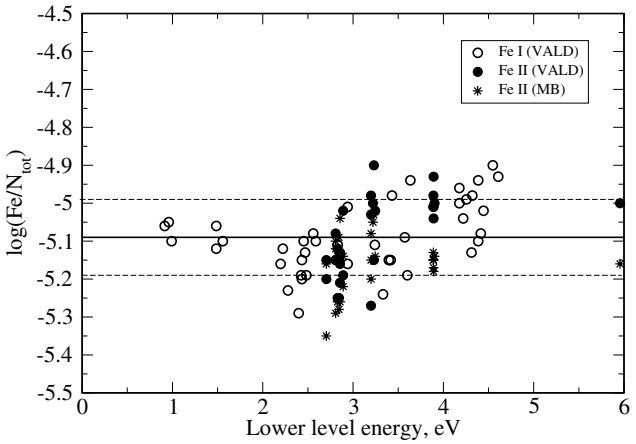

Fig. 2. Iron abundance based on NLTE calculations versus lower level energy. Individual abundances from Fe I (open circles), Fe II (VALD oscillator strengths – filled circles) and Fe II (Meléndez & Barbuy 2003 oscillator strengths – asterisks) are shown. Horizontal lines indicate the mean Fe abundance with ±0.1 deviation.

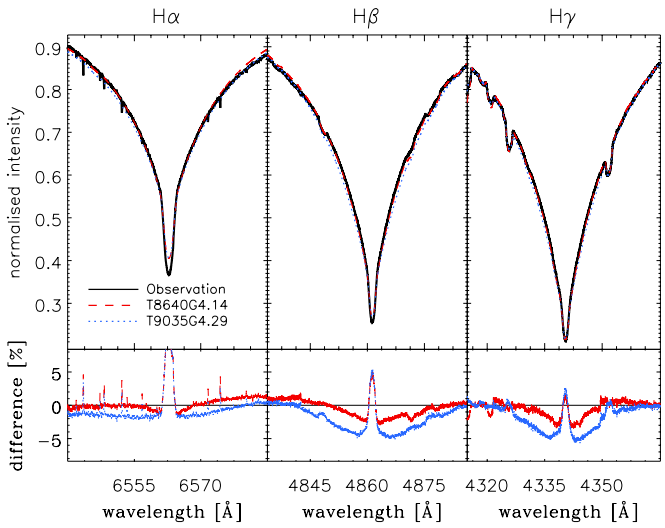

Fig. 3. Region of the Hα (*left*), Hβ (*middle*), and Hγ (*right*) lines for HD 144277: observed spectra (solid black line), synthetic spectra with the final adopted stellar parameters ($T_{\rm eff}$ = 8640 K, $\log g$ = 4.14; solid red line) and synthetic spectra using the $T_{\rm eff}$ and $\log g$ values derived from fitting the spectral regions excluding the Balmer lines (i.e., $T_{\rm eff}$ = 9035 K, $\log g$ = 4.29; dashed blue lines). The *lower panels* show the differences (in %) between observed and synthetic spectra for the three Balmer line regions.

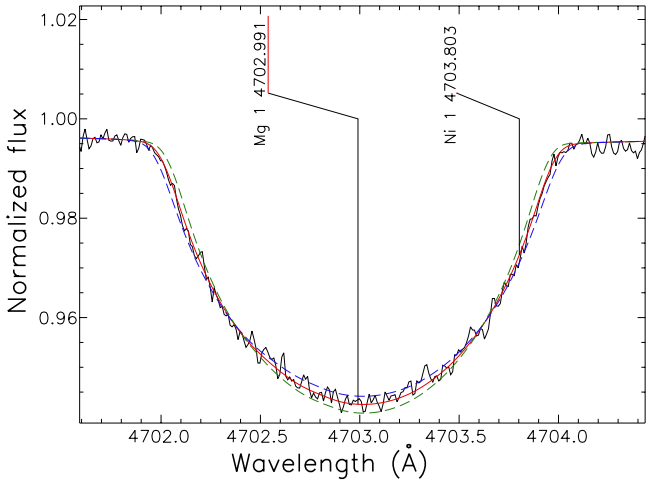

Fig. 4. Zoom into the region of the Mg I line at 4702 Å: observed spectrum (solid black line), synthetic spectrum with the best fitting $\upsilon \sin i$ value of 62 km s^{-1} (solid red line) and two synthetic spectra calculated by increasing and decreasing $\upsilon \sin i$ by 2 km s^{-1} (dashed blue and green lines).

used only the three Balmer lines as input for SME; (ii) we took the spectral regions without the Balmer lines; and (iii) all above-mentioned spectral regions were selected at the same time. The corresponding solutions are 8558 K/4.15/−0.56 (i), 9035 K/4.29/−0.33 (ii) and 8641 K/4.14/−0.54 (iii) for $T_{\rm eff}$, $\log g$, and metallicity [Fe/H]. All three solutions give $\upsilon \sin i$ values close to 62 km s^{-1}. Microturbulent velocity varied around 2.5 km s^{-1}. In the temperature region of the assumed position of HD 144277, the hydrogen lines are rather insensitive to variations in $T_{\rm eff}$ and more sensitive to variations in $\log g$, while the ionization balance for Fe I/Fe II is sensitive both to $T_{\rm eff}$ and $\log g$. The use of the ionization balance requires accurate transition probabilities for Fe I and Fe II lines as well as non-local thermodynamic equilibrium (NLTE) line formation.

We applied an extensive model atom of Fe I and Fe II from Mashonkina (2011a). NLTE level populations were calculated using a revised version of the DETAIL code developed by Butler and Giddings (1985). NLTE leads to a weakening of the Fe I lines, and the NLTE abundance corrections vary from 0.00 to +0.09 dex. For the Fe II lines, the NLTE abundance corrections are negative and do not exceed 0.01 dex in absolute value. The iron abundance computed from the Fe II lines depends on the adopted system of the oscillator strengths. Figure 2 shows the abundances derived from NLTE calculations of the Fe I and Fe II lines with different oscillator strengths taken from VALD and from Meléndez & Barbuy (2003). While both sets provide reasonable agreement for the lines with the excitation potential <3.5 eV, a difference ~0.1 dex appears for the lines with the excitation potential >3.8 eV. As a reasonable compromise we therefore adopted the final parameters for HD 144277 as $T_{\rm eff} = 8640^{+300}_{-100}$ K, $\log g = 4.14 \pm 0.15$, $\upsilon_{\rm mic}$ =2.5 ± 0.3 km s^{-1}, and $\upsilon \sin i = 62 \pm 2$ km s^{-1}. Errors for $T_{\rm eff}$ are computed with SME using different spectral regions and for $\log g$ by allowing ± 0.1 dex difference in the Fe I/Fe II ionization balance. A comparison between the observed and calculated line profiles for Hα, Hβ, and Hγ is shown in Fig. 3. A zoom into the Mg I line at 4702 Å (Fig. 4) illustrates the accuracy of the $\upsilon \sin i$ determination.

Table 1 lists the element abundances in the atmosphere of HD 144277 with their standard deviations. The most realistic estimate of the error comes from the Fe lines because it is the only element with a statistically significant number of lines. For a few elements other than Fe, abundances were also derived taking NLTE effects into account. For example, the oxygen abundance was calculated following the procedure described by Sitnova et al. (2013).

Our model provides us with an ionization equilibrium for Fe (see above), Mg and Ca. The Mg abundance from Mg I lines was derived using NLTE calculations by Mashonkina (2013). The Mg abundance in LTE computed from the Mg II lines was derived using the two lines at 4390.5 and 4481.2 Å.

The NLTE formation of Mg II lines in the atmospheres of three A-type stars was studied by Przybilla et al. (2001); two models were computed for supergiants, and the third model is for a main sequence star of $T_{\rm eff}$ = 9550 K and $\log g$ = 3.95. The

Table 1. LTE atmospheric abundances in HD 144277 with the error estimates based on the internal scattering from the number of analysed lines, n.

Ion	HD 144277			Sun
	$\log(N_{el}/N_{tot})$	n	$[(N_{el}]$	$\log(N_{el}/N_{tot})$
He I	−1.05:	1	0.06	−1.11
C I	−3.68 ± 0.08	8	-0.07	−3.61
O I *	−3.34 ± 0.06	3	0.01	−3.35
Mg I*	−4.94 ± 0.11	5	-0.50	−4.44
Mg II*	−4.92 ± 0.05	2	-0.48	−4.44
Si II	−5.02 ± 0.03	4	-0.49	−4.53
S I	−4.99 ± 0.14	5	-0.07	−4.92
Ca I*	−6.23 ± 0.06	10	-0.53	−5.70
Ca II*	−6.24 ± 0.07	3	-0.54	−5.70
Sc II	−9.49 ± 0.04	3	-0.60	−8.89
Ti II	−7.62 ± 0.12	13	-0.53	−7.09
Cr I	−7.05 ± 0.09	5	-0.65	−6.40
Cr II	−6.91 ± 0.06	10	-0.51	−6.40
Fe I*	−5.09 ± 0.09	40	-0.55	−4.54
Fe II*	−5.09 ± 0.10	29	-0.55	−4.54
Ni I	−6.38 ± 0.10	3	-0.56	−5.82
Sr II	−9.82 ± 0.08	2	-0.65	−9.17
Y II	−10.43 ± 0.10	2	-0.60	−9.83
Ba II	−10.53 ± 0.10	4	-0.67	−9.86

Notes. Elements treated in NLTE are marked by asterisks. $[(N_{el}/N_{tot})]$ is the abundance of a certain element relative to the total abundance of all elements, which is set to be equal to 1. For purpose of comparison, the last column gives the abundances of the solar atmosphere calculated by Asplund et al. (2009).

effective temperature of this 1D model is hotter by 900 K than that of HD 144277, but model atmospheres for both stars have comparable gravity and metallicity. Hence, we can apply these theoretical calculations to estimate possible NLTE corrections for HD 144277.

In the model atmosphere of a star with T_{eff} = 9550 K and $\log g = 3.95$, the line at 4390 Å is not affected by NLTE while the NLTE correction is −0.2 dex for the 4481.2 Å line (Przybilla et al. 2001). The Mg abundance inferred from the 4390 Å line is $\log(Mg/N_{tot}) = -4.88$. Applying this correction to $\log(Mg/N_{tot}) = -4.75$ derived from the 4481.2 Å line, we estimate an average Mg abundance of −4.92 ± 0.05 from NLTE calculations that agrees well with the Mg abundance derived from the NLTE analysis of the Mg I lines.

The Ca I, Ca II abundances were calculated for the atmosphere of HD 144277 in NLTE with the model atom from Mashonkina, Korn & Przybilla (2007). For the Cr II lines we used the most recent transition probability calculations by Kurucz[1] that provide reasonable agreement with the abundances derived from Cr I lines.

HD 144277 has solar chemical composition for the light elements C, O, Na, and S, but shows underabundances in the heavier elements. The average metallicity calculated from the elements Si to Ba is $M = -0.40 \pm 0.14$. If we include in the metallicity calculations all those species (C to Ba) for which we derived abundances, then we get a Z value of 0.011. The He abundance was measured only from a single line (see Table 1), but seems to be slightly higher than the solar value, i.e., by 0.04. In turn, this affects the X value to be 0.72 instead of 0.74 as in the solar case (see Table 2).

Figure 5 shows the fit of the synthetic fluxes, calculated with the fundamental parameters derived by us, to the observed TD1

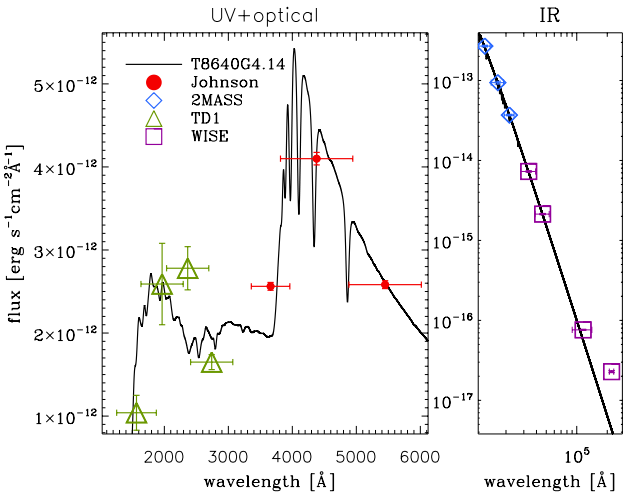

Fig. 5. Comparison between LLMODELS theoretical fluxes (thick black line), calculated with the fundamental parameters derived for HD 144277 (T_{eff} = 8640 K, $\log g$ = 4.14), and observed Johnson (crosses), 2MASS (diamonds), TD1 (triangles), and WISE (squares) photometry converted to physical units.

Table 2. Parameters of asteroseismic models of HD 144277 and comparison with the results from spectroscopy.

	Model 2 (Paper I)	Model 3	Spectroscopy
X	0.70	0.70	0.72
Z	0.010	0.011	0.011
$M/M_\odot$	1.66	1.70	1.72
$\log T_{eff}$	3.9407	3.9404	3.94 ± 0.01
$\log L/L_\odot$	1.04	1.05	$1.09^{+0.38}_{-0.53}$
$R/R_\odot$	1.456	1.469	1.56 ± 0.69
$\log g$	4.332	4.325	4.14 ± 0.15
V_{rot} [km s^{-1}]	15.0	79.7	($v \sin i$:) 62.0 ± 2.0

(Thompson et al. 1992), Johnson (Myers et al. 2002), 2MASS (Cutri 2003), and WISE (Cutri et al. 2012) photometry, converted to physical units. Calibrations by Bessel et al. (1998), van der Bliek et al. (1996), and Wright et al. (2010) were used for Johnson, 2MASS, and WISE photometry, respectively. The distance of 143 ± 63 pc was taken from Kharchenko & Roeser (2009) and the interstellar reddening $E(B-V) = 0.01$ mag from Amores & Lepine (2005). The best fit was achieved for a stellar radius of $R = 1.56 \pm 0.69\,R_\odot$; the relatively large error is mainly caused by the large uncertainty in distance.

For T_{eff} = 8640 K and $\log g$ of 4.14 an increase in gravity on the order of 0.15 dex results in a violation of the Fe I/Fe II ionization balance exceeding the expected NLTE effects by a factor of two. We therefore take $\log g = 4.3$ as a real upper limit. With the T_{eff} = 8640 K derived from the spectrum analysis and the radius of 1.56 $R_\odot$, we estimate HD 144277's luminosity to be $\log L/L_\odot = 1.09^{+0.38}_{-0.53}$. The uncertainties in luminosity can only be used as formal errors that fully take the uncertainty of the distance into account. As HD 144277 is certainly not a sub-dwarf, its radius must at least be larger than the solar radius. This would decrease the real lower error bar on the radius to 0.56 $R_\odot$ and on the luminosity to 0.41.

A summary of the observationally determined values can be found in the third column of Table 2.

[1] http://kurucz.harvard.edu/atoms/2401/

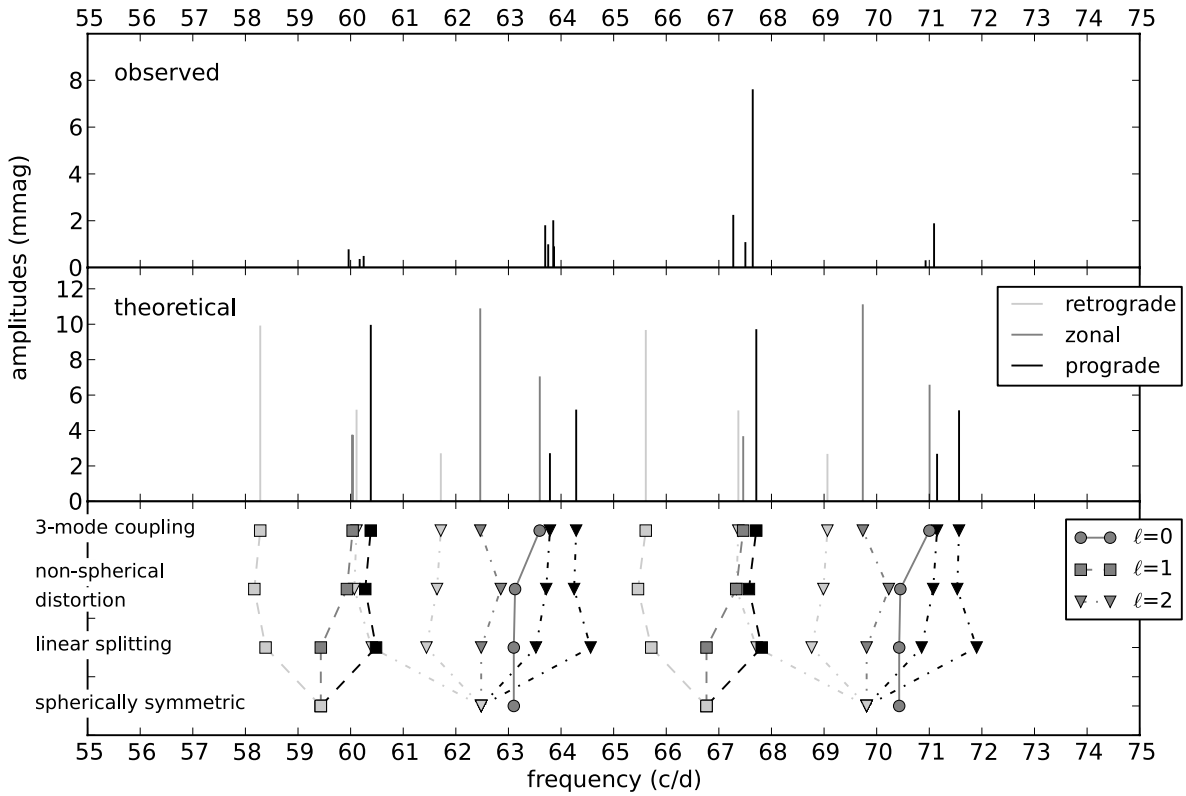

Fig. 6. *Top panel*: observed modes. *Middle panel*: theoretical modes with $\ell \leq 2$: retrograde (light grey), zonal (dark grey), and prograde (black) modes. *Lower panel*: stepwise addition of various rotational effects on the mode frequencies in near-degenerate mode perturbation theory (spherical symmetry, linear splitting, non-spherical distortion, and three-mode coupling). Only $\ell = 0, 1, 2$ are shown for clarity as filled circles, squares, and triangles.

4. Refinement of the asteroseismic model

The asteroseismic model presented in Paper I was mainly derived based on information extracted from the observed frequency spectrum. With our new spectroscopic observations, we gained additional constraints on the fundamental parameters of the star. Consequently, the asteroseismic model can now be tested and possibly refined.

The new observations could confirm a lower metallicity compared to solar composition, which was predicted by the asteroseismic models in Paper I in order to explain the pulsational instability of the observed modes. The spectroscopically determined temperature, luminosity, and radius agree within one sigma to the values derived from asteroseismology, whereas the theoretical and spectroscopical log g values match only within 2σ (see Table 2). On the other hand, spectroscopy indicates that with $v \sin i = 62.0 \pm 2.0\,\mathrm{km\,s^{-1}}$ the rotational velocity of HD 144277 is higher than assumed in the asteroseismic models in Paper I, where an equatorial rotation velocity of $15\,\mathrm{km\,s^{-1}}$ was adopted. Since most fundamental parameters of the original asteroseismic model are in good agreement with the new observations, we used Model 2 from Paper I as a reference model (see Table 2) and increased its rotational velocity to study the influence on the predicted frequencies and mode instability.

To estimate the effects of rotation on the frequencies we used a second-order perturbation theory, which is sufficient only for reasonably slow rotators. Increasing the rotational velocity at the equator from $15\,\mathrm{km\,s^{-1}}$ to $60\,\mathrm{km\,s^{-1}}$ implies that the effects of near-degeneracies gain importance. As shown in, e.g., Goupil et al. (2000) modes can couple if (i) they are close in frequency; (ii) their spherical degree differs by 2; and (iii) their azimuthal orders are equal. We therefore also considered the effects of rotational mode coupling according to the formalism presented in Soufi et al. (1998) and Daszyńska-Daszkiewicz et al. (2002). In our study we considered the rotational coupling of up to three modes and conducted tests thereby adopting various values for the rotational velocity. The adopted evolutionary and pulsational codes were the same as those used in Paper I. We again used OPAL opacities (Iglesias & Rogers, 1996) and the Asplund et al. (2009) proportions in the heavy element abundances to be consistent with Paper I.

We find that the best agreement between observational and theoretical frequencies is found if we assume a rotational velocity at the equator between 60 and $80\,\mathrm{km\,s^{-1}}$. For higher rotation there are no clear patterns in the theoretical frequency spectra that can be matched to the very regular pattern of the observed frequencies. This finding implies a nearly equator-on view. As can be seen in Fig. 6, the observed groups of frequencies at 60 and $67\,\mathrm{d^{-1}}$ correspond to prograde and zonal dipole modes, while the other two groups are related to the radial and quadrupole modes.

Table 2 presents a comparison between the fundamental parameters of Model 2 from Paper I and the new model presented in this paper (denoted as Model 3). The position of the model in the Hertzsprung-Russell (HR) diagram is shown in Fig. 7. For the refined asteroseismic model a small increase in the metallicity was adopted to improve the agreement between the instability of theoretical modes and observed unstable modes (see Fig. 8). However, with $Z = 0.011$ the model remains clearly metal underabundant compared to the solar value of $Z = 0.0134$ (Asplund et al. 2009).

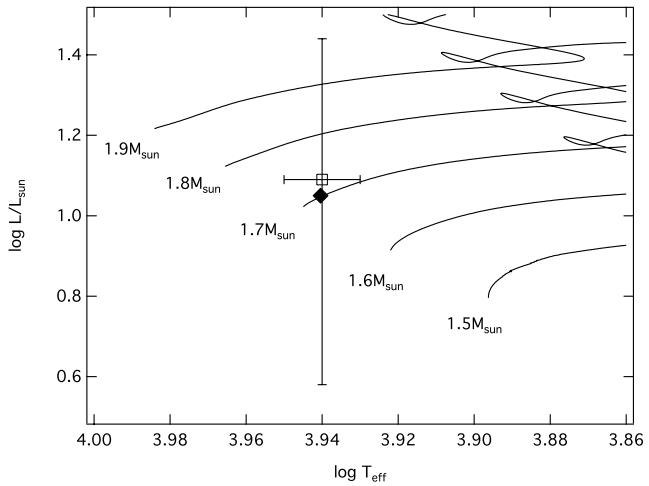

Fig. 7. HD 144277 in the HR-diagram: post-main sequence evolutionary tracks (solid lines) for 1.5 to 1.9 $M_\odot$ in steps of 0.1 $M_\odot$ computed for the same chemical composition (X, Z) as indicated by spectroscopy and by asteroseismology, refined asteroseismic model (solid diamond), and observational position (open square) of HD 144277.

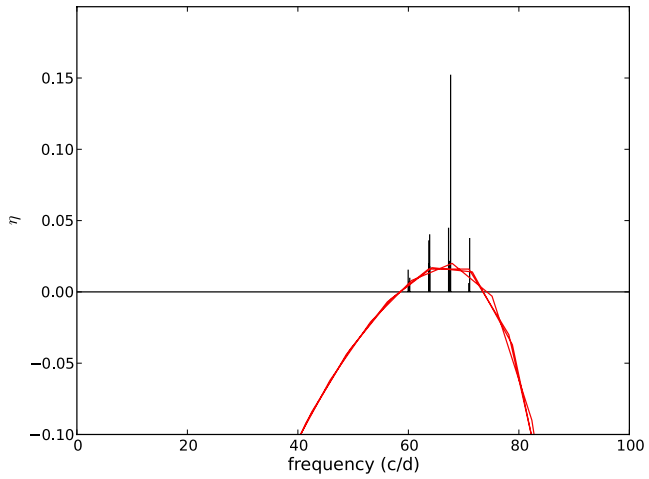

Fig. 8. Instability parameter, $\eta = \int_0^R (\mathrm{d}W/\mathrm{d}r)\mathrm{d}r / \int_0^R |\mathrm{d}W/\mathrm{d}r|$, vs. mode frequency. Positive η corresponds to driven modes. Observed modes are shown with vertical lines. The two (red) lines show the value of the instability parameter for $\ell = 1$ and 2.

For stars with fundamental parameters similar to HD 144277, the theory does not expect significant convective core overshooting. Indeed no overshooting is needed to derive the asteroseismic model presented in this paper; however, HD 144277 is too young for its observed frequencies and fundamental parameters to impose any real constraints on core overshooting to the model.

5. Summary and conclusions

Our first asteroseismic model for HD 144277 was based solely on the observed pulsation frequency spectrum (see Paper I) since no high-resolution spectroscopy was available. This first model predicted a slightly less than solar metallicity and assumed a rotational velocity at the equator of only 15 km s^{-1}.

Using the high-resolution, high S/N HARPS spectra we confirmed the slightly less than solar metallicity needed to excite the observed δ Scuti frequencies in the range of 59.9 to 71.1 d^{-1} (see Paper I). The fundamental parameters $T_{\rm eff}$, $\log g$, $\log L/L_\odot$, and $R/R_\odot$ determined by spectroscopy agree within one sigma with the values found by asteroseismology.

The major difference between the assumptions used in our first asteroseismic models and the spectroscopically derived values for HD 144277 is the rotational velocity. While we assumed a rotational velocity at the equator of 15 km s^{-1} in our first analysis, the projected rotational velocity, $\upsilon \sin i$, is significantly higher at 62.0 ± 2.0 km s^{-1}. In the present study we therefore included effects of near-degeneracies and rotational mode coupling of up to three modes.

As the best agreement between the observed and theoretical pulsation frequencies is found for a rotational velocity at the equator of about 80 km s^{-1}, the star has to be seen equator-on.

A near equator-on view implies that zonal modes have lower visibility than prograde and retrograde modes for geometrical reasons (see, e.g., Fig. 6 in Breger & Lenz 2008). Our asteroseismic model indicates that the observed frequencies are prograde modes. Consequently, the following question arises: why are the retrograde dipole modes not observed, despite their having a similar geometrical visibility to the prograde modes? A striking feature that may be the key to the physical mechanism of mode selection in the special case of HD 144277 is that we particularly see those modes that are very close in frequency and affected by rotational mode coupling. These modes are in the center panel of Fig. 6 so that a better comparison can be made with the theoretical mode distribution shown in the panel below and observations on top. This good agreement indicates that HD 144277 may give us a valuable hint as to how the mode selection works in young δ Scuti stars.

Acknowledgements. The authors would like to thank our referee, Torsten Böhm, for his valuable comments that helped to improve the paper significantly. We thank L. Mashonkina for providing us with the departure coefficients for the Mg NLTE analysis. The research leading to these results has received funding from the European Research Council under the European Community's Seventh Framework Programme (FP7/2007–2013)/ERC grant agreement No. 227224 (PROSPERITY). This research is (partially) funded by the Research Council of the KU Leuven under grant agreement GOA/2013/012. The research leading to these results was also based on funding from the Fund for Scientific Research of Flanders (FWO), Belgium, under grant agreement G.0B69.13. K.Z. and M.B. acknowledge support from the Austrian Fonds zur Förderung der wissenschaftlichen Forschung (project P21830-N16). T.R. acknowledges partial financial support from Basic Research Program of the Russian Academy of Sciences "Origin and Evolution of Stars and Galaxies". A.A.P. acknowledges partial financial support from the Polish NCN grant No. 2011/01/B/ST9/05448. The INAF-OA Brera team acknowledges financial support from the PRIN-INAF 2010 Asteroseismology: looking inside the stars with space- and ground-based observations. M.R. also acknowledges financial support from the FP7 project SPACEINN: Exploitation of Space Data for Innovative Helio- and Asteroseismology. M.H. acknowledges support from the Austrian Fonds zur Förderung der wissenschaftlichen Forschung (project P22691-N16).

References

Amôres, E. B., & Lépine, J. R. D. 2005, AJ, 130, 659
Asplund, M., Grevesse, N., Sauval, A. J., & Scott, P. 2009, ARA&A, 47, 481
Balona, L. A. 1994, MNRAS, 268, 119
Bessel, M.S., Castelli, F., & Plez, B. 1998, A&A, 333, 231
Breger, M., & Lenz, P. 2008, A&A, 488, 643
Butler, K., & Giddings, J. 1985, Newsletter on Analysis of Astronomical Spectra (University of London), 9, 723
Cutri, R. M., Skrutskie, M. F., van Dyk, S., et al. 2003, The IRSA 2MASS All-Sky Point Source Catalog (NASA/IPAC Infrared Science Archive; http://irsa.ipac.caltech.edu/applications/Gator/)
Cutri, R. M., et al. 2012, WISE All-Sky Data Release, VizieR Online Data Catalog: II/311
Daszyńska-Daszkiewicz, J., Dziembowski, W. A., Pamyatnykh, A. A., & Goupil, M.-J. 2002, A&A, 392, 151

Goupil, M.-J., Dziembowski, W. A., Pamyatnykh, A. A., & Talon, S. 2000, ASP Conf. Ser., 210, 267
Iglesias, C. A., & Rogers, F. J. 1996, ApJ, 464, 943
Kaiser, A. 2006, in Astrophysics of Variable Stars, eds. C. Sterken, & C. Aerts, ASP Conf. Ser., 349, 257
Kharchenko, N. V., & Roeser, S. 2009, Kinematics and Physics of Celestial Bodies, 17, 409
Kochukhov, O. 2007, in Physics of Magnetic Stars: Proc. Int. Conf. Special Astrophysical Observatory, eds. I. I. Romanyuk, & D. O. Kudryavtsev, RAS, 109
Kupka, F., Piskunov, N., Ryabchikova, T. A., Stempels, H. C., & Weiss, W. W. 1999, A&AS, 138, 119
Kurucz, R. 1993, ATLAS9: Stellar Atmosphere Programs and 2 km s^{-1} grid. Kurucz CD-ROM No. 13 (Cambridge: Smithsonian Astrophysical Observatory)
Mashonkina, L. 2011, in Physics of Magnetic Stars, Proc. Int. Conf. Special Astrophysical Observatory, RAS, eds. I. I. Romanyuk, & D. O. Kudryavtsev, 314
Mashonkina, L. 2013, A&A, 550, A28
Mashonkina, L., Korn, A. J., & Przybilla, N. 2007, A&A, 461, 261
Mayor, M., Pepe, F., Queloz, D., et al. 2003, The Messenger, 114, 20
Meléndez, J., & Barbuy, B. 2009, A&A, 497, 611
Moon, T. T., & Dworetsky, M. M. 1985, MNRAS, 217, 305
Myers, J. R., Sande, C. B., Miller, A. C., Warren, Jr. W. H., & Tracewell, D. A. 2002, SKY2000 Master Catalog, 4th version, VizieR Online Data Catalog: V/105
Przybilla, N., Butler, K., Becker, S. R., & Kudritzki, R. P. 2001, A&A, 369, 1009
Rainer, M. 2003, Laurea Thesis, Università degli Studi di Milano, Italy
Ribas, I., Jordi, C., Torra, J., & Gimenez, A. 1997, A&A, 327, 207
Shulyak, D., Tsymbal, V., Ryabchikova, T., Stütz Ch., & Weiss, W. W. 2004, A&A, 428, 993
Sitnova, T., Mashonkina, L., & Ryabchikova, T. 2013, Astron. lett., 39, 126
Soufi, F., Goupil, M. J., & Dziembowski, W. A. 1998, A&A, 334, 911
Thompson, G. I., Nandy, K., Jamar, C., et al. 1992, Catalogue of stellar ultraviolet fluxes, VizieR Online Data Catalog: V/38
Tkachenko, A., Lehmann, H., Smalley, B., Debosscher, J., & Aerts, C. 2012, MNRAS, 422, 2960
Tsymbal, V. V. 1996, in Model Atmospheres and Spectral Synthesis, eds. S. J. Adelman, F. Kupka, & W. W. Weiss, ASP Conf. Ser., 108, 198
Valenti, J. A., & Fischer, D. A. 2005, ApJS, 159, 141
Valenti, J. A., & Piskunov, N. 1996, A&AS, 118, 595
van der Bliek, N. S., Manfroid, J., & Bouchet, P. 1996, A&AS, 119, 547
Walker, G., Matthews, J. M., Kuschnig, R., et al. 2003, PASP, 115, 1023
Wright, C. O., Egan, M. P., Kraemer, K. E., & Price, S. D. 2003, AJ, 125, 359
Wright, E. L., Eisenhardt, P. R. M., Mainzer, A. K., et al. 2010, AJ, 140, 1868
Zwintz, K., Lenz, P., Breger, M., et al. 2011, A&A, 533, A133